Atomic Sensors – A Review

John Kitching, Svenja Knappe, and Elizabeth A. Donley

(Invited Paper)

***Abstract*—We discuss the basic physics and instrumentation issues related to high-performance physical and inertial sensors based on atomic spectroscopy. Recent work on atomic magnetometers, NMR gyroscopes, and atom interferometers is reviewed, with a focus on precision sensing of electromagnetic and gravitational fields and inertial motion. Atomic sensors have growing relevance to many facets of modern science and technology, from understanding the human brain to enabling precision navigation of moving platforms.**

***Index Terms*—Atomic spectroscopy, inertial sensor, magnetometry.**

I. Introduction

ATOMIC spectroscopy is the basis for many precise measurements of physical quantities. The second, for example, is currently defined in terms of a microwave transition in a $^{133}\mathrm{Cs}$ atom, and can be realized with an accuracy better than 1 part in 10^{15} via microwave spectroscopy in an atomic frequency standard. Because spectroscopy of this type can be so precise, and because many physical phenomena (electromagnetic fields, for example) affect the atomic structure that gives rise to the spectroscopic signals, sensors with high performance are possible. For example, atomic (optical) magnetometers with a sensitivity below 1 $\mathrm{fT}/\sqrt{\mathrm{Hz}}$ have recently been demonstrated [1], as have nuclear magnetic resonances (NMR) gyroscopes with an angle-random walk (ARW) below 0.01 $\mathrm{deg}/\sqrt{\mathrm{h}}$ [2].

Most atomic sensors are based on a pair of discrete energy states in the atom and can be understood as proceeding in three steps (see Fig. 1). First, the atoms are prepared in a well-defined state. This state could be a spin orientation with respect to an external magnetic field, for example, or an energy state related to the internal structure of the atoms (a specific hyperfine state, for example). The state of the atoms then evolves in the presence of the field to be measured. Finally, the altered state of the atom is measured and the effects of the presence of the field are deduced.

Manuscript received March 21, 2011; revised May 17, 2011; accepted May 18, 2011. Date of publication May 27, 2011; date of current version July 27, 2011. This work was supported in part by the National Institute of Standards and Technology (NIST) and the Defense Advanced Research Projects Agency (DARPA). The associate editor coordinating the review of this paper and approving it for publication was Dr. John Vig.

J. Kitching and E. A. Donley are with the National Institute of Standards and Technology, Boulder, CO 80305 USA (e-mail: john.kitching@nist.gov; elizabeth.donley@nist.gov).

S. Knappe is with the National Institute of Standards and Technology, Boulder, CO 80305 USA and the University of Colorado, Boulder, CO 80309 USA (e-mail: svenja.knappe@nist.gov).

Color versions of one or more of the figures in this paper are available online at http://ieeexplore.ieee.org.

Digital Object Identifier 10.1109/JSEN.2011.2157679

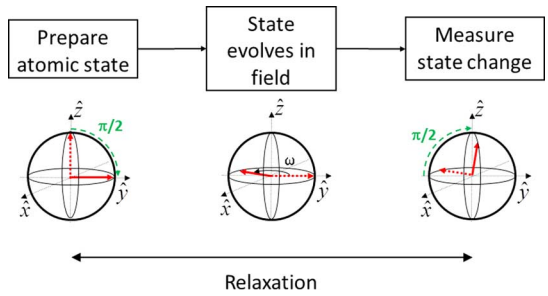

Fig. 1. Sensing fields by use of atoms. The measurement is represented in three steps in the Bloch sphere picture. First, atoms are prepared in a well-defined state that is sensitive to the field F to be measured. Then, the state evolves at a frequency $\omega_0 = \mu F/\hbar$ for a time limited by relaxation processes. The final state is then measured and the effects of the field are deduced. Often, only an eigenstate of the interaction Hamiltonian (oriented here along z) can be prepared and detected; this state is insensitive to the field. In this case, the initial eigenstate can be transformed into a state maximally sensitive to the field (and back again into the detection basis), by the application of a $\pi/2$ pulse, as described in the text.

States of the atom are typically visualized as the rotation of a vector on the Bloch sphere [3] (see Fig. 1). In the Bloch sphere representation, the two energy eigenstates involved in the interaction are represented by vectors pointing along $+\mathrm{z}$ and $-\mathrm{z}$, respectively. Coherences (oscillating electromagnetic moments) are represented by the transverse component of the vector. The interaction of the atom with the field to measured can be characterized by a transverse phase:

$$\phi_{\mathrm{int}} = \frac{1}{\hbar}\int H_{\mathrm{int}} dt, \tag{1}$$

where $H_{\mathrm{int}} = \mu F \equiv \hbar\omega_0$ is the interaction energy of the atom with the field, $\hbar$ is Planck's constant, ω_0 is the frequency at which the state evolves, and F and μ are the field to be measured and the property of the atom affected by the field, respectively. For example, for an atomic magnetometer, which relies on the precession of a magnetic spin in a magnetic field, μ is the magnetic moment of the atom and F is the magnetic field. In the case of inertial sensors, F is the rotation rate and μ is the angular momentum of the atom.

The state of the atom can be prepared and measured in several ways. Early determination and selection of the spin states of atoms was done using a Stern–Gerlach apparatus; a technique still used in modern commercial atomic clocks based on thermal beams. Optical pumping [4] is often a better alternative, and relies on the use of light fields to prepare the atoms in a well-defined quantum state.

In many state preparation and detection schemes, only the longitudinal component of the Bloch vector (aligned with the z axis in Fig. 1) can be measured. Such a measurement is

TABLE I
PROPERTIES OF SEVERAL TYPES OF ATOMIC SENSORS

Sensor type	T_2 [s]	$\delta\varphi$ [rad] @ T_2	H_{int}	$\omega_0/2\pi$	*Stability or Sensitivity @ 1s*	*Reference*
Ion optical clock	1	~1	$\alpha q_n q_e$	10^{15} Hz	10^{-15}	[7]
Fountain atomic clock	1	10^{-4}	$\beta\vec{\mu}_n\cdot\vec{\mu}_e$	10^{10} Hz	10^{-14}	[8]
Beam atomic clock	0.01	10^{-3}	$\beta\vec{\mu}_n\cdot\vec{\mu}_e$	10^{10} Hz	10^{-12}	[9]
Vapor cell magnetometer	0.01	10^{-4}	$\vec{\mu}\cdot\vec{B}$	10^{10} Hz/T	10^{-13} T	[10]
Vapor cell NMR gyroscope	100	10^{-8}	$\vec{L}\cdot\vec{\Omega}$	7×10^{-7} Hz/(°/h)	10^{-3} °/h	[2]
Laser cooled atom interferometer accel.	1	0.1	$\hbar kTa$	10^{7} Hz/g	10^{-8} g	[11]
Atomic electric field sensor	10^{-7}	~0.1	$\vec{d}\cdot\vec{E}$	10^{8} Hz/(V/cm)	~10 μV/cm	[12]

insensitive to the transverse angle, and additional steps must be added to measure the effects of the field. These steps involve the application of an oscillating field that couples the two atomic levels involved in the Bloch vector representation. The frequency, strength, and duration of the oscillating field can be adjusted to rotate the Bloch vector by an angle $\pi/2$ about a transverse axis on the Bloch sphere (x axis in Fig. 1); such a rotation is known as a $\pi/2$ pulse. An atom initially prepared in a well-defined longitudinal state (pointing up in Fig. 1, for example) is rotated into the transverse plane by the $\pi/2$ pulse, and is then allowed to precess under the influence of the external field to be measured. After the atom precesses for a certain period, a second $\pi/2$ pulse is applied, which results in a final state with a longitudinal component proportional to the transverse phase shift. A subsequent measurement of the longitudinal component therefore measures the transverse phase shift and the corresponding field. This measurement process is analogous to an interferometric measurement of the phase of a wave.

The minimum field that the sensor can measure, $\delta F_{\min}$, is determined by the total phase shift induced by the field and the corresponding phase resolution, $\delta\varphi$, of the measurement method:

$$\delta F_{\min} = \frac{h\delta\varphi}{\mu T}, \tag{2}$$

where T is the time over which the state evolves in the field. For a measurement of N quantum-mechanically uncorrelated atoms with no other noise sources present, $\delta\varphi = \delta\varphi_{SQL} = 1/\sqrt{N}$ [5]. This phase uncertainty arises because of the quantum-mechanical property of the atoms that a measurement will project them into a well-defined quantum state with a probability determined by the amplitude of that state in the atomic wavefunction. The probabilistic nature of the measurement therefore introduces noise, often referred to as "quantum projection noise" or "atom shot noise" [5].

The evolution of the state in the field to be measured is typically contaminated by one or more relaxation mechanisms. Relaxation usually limits the period over which a single measurement of the state phase can be made. Relaxation can be caused by electromagnetic absorptive or radiative processes, collisions, and field gradients. In the absence of relaxation, the measurement period is limited by how long the atoms remain in the apparatus. For example, in fountain atomic clocks, the atoms fall under gravity, and the measurement period is therefore limited to about 1 s in an apparatus of height 1 meter.

In the presence of relaxation, (1) is valid only when the measurement time T is much less than the characteristic relaxation time T_2. For $T > T_2$, the sensitivity is given by the incoherent sum of (T/T_2) independent measurements of time T_2 each:

$$\delta F_{\min} = \frac{h\delta\varphi}{\mu T_2}\sqrt{\frac{T_2}{T}} = \frac{h}{\mu\sqrt{T_2 T N}}, \tag{3}$$

where the last equality assumes a phase resolution corresponding to quantum projection noise on N uncorrelated atoms. For example, in the case where F is a magnetic field and μ is the magnetic moment of the atoms, (2) reduces to the basic expression for the atom-shot-noise-limited sensitivity of a magnetometer [6].

Atomic sensors can be implemented in a number of ways, depending on the quantity to be measured and the required precision. The main methods for confining the atoms are in a sealed cell at room temperature, by laser cooling the atoms to microkelvin temperatures, or by confining them with electromagnetic fields. In a room-temperature vapor cell, more atoms can be probed, but the relaxation is typically stronger than in the other methods due to more rapid collisions with the walls of the cell. A summary of some common types of atomic sensors is shown in Table I.

II. ATOMIC CLOCKS

Atomic clocks [13] can be thought of as atomic sensors, in which an electron in the atom is sensing the electric or magnetic field produced by the nucleus. While they do not, strictly speaking, function as sensors, atomic clocks share many properties with more typical atomic sensors and hence serve as a useful illustrative example [14]. Time has been the most precisely measured physical quantity for many years because of the exquisite precision routinely achieved by these instruments.

An atomic clock is based on electromagnetic coherences (oscillations) related to the internal state of an atom. Microwave atomic clocks [13] are based on hyperfine interactions in atoms with nonzero nuclear spin, which result from the interaction of the nuclear magnetic moment with the magnetic field caused by the valence electron [see Fig. 2(a)]. The interaction energy is proportional to the product $\mu_n\mu_e$ of the nuclear and electron magnetic moments, and corresponds to a transition frequency ω_0 of about 2π (10 GHz). Atoms in a microwave clock are prepared in a well-defined hyperfine energy level with magnetic state selection or optical pumping. The hyperfine coherence is

then excited by applying a resonant microwave field as a $\pi/2$ pulse. After a period of time in free flight, a second $\pi/2$ pulse is applied and the population in each hyperfine level is measured. Ramsey fringes are measured as a function of microwave frequency and can be used to lock the microwave oscillator to the atomic transition.

Fountain clocks [15],[16], the most accurate instruments at present for realizing the SI second, have interaction times T of about 1 s, as mentioned above. Radiative relaxation is very weak for these magnetic dipole transitions and does not contribute significantly to the achievable measurement time. These instruments often reach a phase resolution $\delta\varphi$ limited by shot noise on the atoms: $1/\sqrt{N}$. The total launched atom number is limited to about 10^8 by technical details of the laser-cooling process and by the need to reduce collisional shifts, which leads to a fractional frequency instability that approaches $\delta\varphi/(\omega_0 T) \sim 10^{-14}$ at 1 s of integration [17].

Optical frequency references [18], such as those based on neutral atoms or ions, achieve higher stability (and, ultimately, overall frequency uncertainty) through an increase in the interaction energy $\hbar\omega_0$. The use of electronic transitions in atoms results in transition frequencies ω_0 in the range of 2π (100 THz) that can be excited by laser fields [see Fig. 2(b)]. Optical frequency references typically involve far fewer atoms than microwave frequency references; ion-based optical [7], for example, often use a single laser-cooled ion probed over an interaction time of 1 s. In this case, the phase error $\delta\varphi$ on each measurement is on the order of unity, but the vastly improved transition frequency still results in better overall stability, approaching 10^{-15} at 1 s [19]. Improvements in the stability of optical clocks may be achieved in the future by increasing the number of ions probed ($N \gg 1$) or by using ensembles of optically trapped neutral atoms [20] with equivalently long relaxation times.

For measuring time intervals longer than about 1 s, atomic clocks vastly outperform other types of clocks, such as those based on mechanical resonances (quartz crystal oscillators) or macroscopic electromagnetic fields (RF cavities). This is essentially because appropriately interrogated single atoms, unlike bulk materials, can be made largely insensitive to specific environmental effects such as temperature that dominate the frequency instability over long time periods. The essence of this environmental insensitivity that is so critical for atomic clocks is also one reason atoms can be made to be such good sensors of other quantities: by reconfiguring the measurement for maximal sensitivity to a field, the effects of all other environmental changes can remain equally small, resulting in a high sensitivity to the field of interest.

III. Atomic Magnetometers

Most atomic magnetometers rely on the measurement of atomic spin evolution in a magnetic field after an overall orientation of the spins is created by optical pumping.

Electrons, as well as many atomic nuclei, have both spin angular momentum and a magnetic dipole moment μ oriented along the spin axis. These two properties lead to the well-known Larmor precession, in which the orientation of

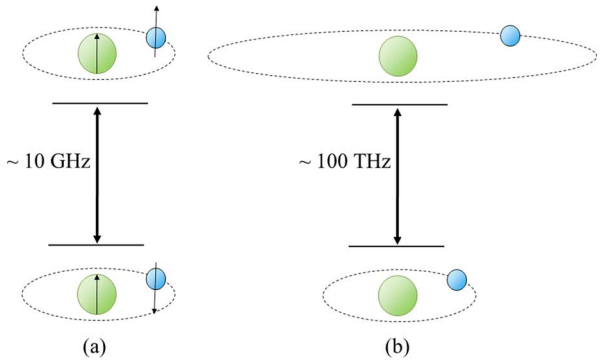

Fig. 2. Energy levels in an atomic clock. (a) Microwave clocks are based on transitions between states that differ in the relative orientation of the electron magnetic moment and the nuclear magnetic moment. (b) Optical clocks are based on transitions between different electron orbitals.

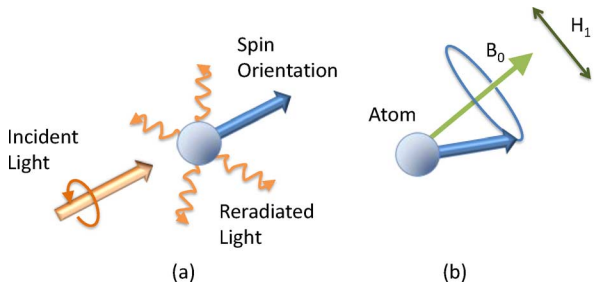

Fig. 3. (a) Optical pumping with circularly polarized light orients the atomic spin parallel to the light direction. (b) Larmor precession of an atomic spin about the magnetic field B_0, driven with a transverse oscillating field H_1.

the particle spin precesses about the magnetic field with a frequency equal to $\omega_0 = \omega_L = \gamma B_0$. Here, B_0 is the magnitude of the local magnetic field and γ is the gyromagnetic constant of the particle, equal to the ratio of its magnetic moment to its angular momentum. As can be seen from Table I, the interaction Hamiltonian describing the system is $H_{\mathrm{int}} = \vec{\mu} \cdot \vec{B}$. Furthermore, the minimum detectable field of an atomic magnetometer is given by (3). If the relaxation time T_2 is dominated by spin-exchange collisions between alkali atoms, for example, the sensitivity limit of the magnetometer can be calculated to be $0.6\ \mathrm{fT/Hz^{1/2}cm^{3/2}}$ [21], depending on the volume V of the vapor cell like $V^{-1/2}$.

In order to create a coherent precession of an ensemble of atoms, the spins first need to be aligned. The angular momentum of atoms can be reoriented by illuminating them with a circularly polarized optical field resonant with an optical (electronic) transition in the atoms [22], as shown in Fig. 3(a). In this particular optical pumping process, an unpolarized atom absorbs the polarized radiation, which has angular momentum with respect to the propagation axis of the light, and re-emits unpolarized radiation isotropically. As a result, the atom gains angular momentum and eventually becomes polarized along the direction of propagation of the optical field. Optical pumping of alkali atoms can be accomplished with an alkali discharge lamp, or with a laser tuned into resonance with an optical transition in the atom. Collisions between a polarized atomic species and an unpolarized species can lead to a transfer of the polarization between one and the other, since the atoms can exchange their spins under collisions. For example, the nuclei of noble gas

atoms can be polarized via spin-exchange collisions with optically polarized alkali atoms contained in the same cell [23].

Atomic magnetometers are usually operated in the continuously driven mode described above. The Larmor precession of the polarized atoms about a magnetic field is driven either directly with an oscillating magnetic field [24], or indirectly with a modulated optical field [25]. When the drive frequency is near resonance with the Larmor frequency, an oscillating atomic polarization is excited, that is phase-coherent with the drive, as shown in Fig. 3(b). While the oscillating polarization generates a corresponding magnetic field that can be directly detected with a coil (as in nuclear magnetic resonance, for example), the polarization in most atomic sensors is detected optically by monitoring the change in power transmitted through the cell or (equivalently) the fluorescence from the atoms [26]. Optical detection can achieve very high signal-to-noise ratios (approaching 10^8 at 1 s of integration) and results in a correspondingly high sensitivity.

The origin of the atomic spin in a magnetometer can be either the spin of an unpaired electron coupled strongly to the nuclear spin (as in alkali atoms) or the intrinsic spin of the nucleus itself, if there are no unpaired electrons. Because of their much lower magnetic moment, nuclear spins precess at a frequency (tens of MHz/T) approximately 1000 times lower than electron spins (tens of GHz/T). Proton magnetometers [27] are a type of nuclear magnetometer based on the precession of the spins of protons in water, kerosene, or ^{3}He. The nuclei are polarized by use of the Overhauser effect [28], where nuclear spin-polarization is transferred between two species of nuclei through cross-relaxation. The spin precession is measured by use of an inductive coil detector. The sensitivity of commercial proton magnetometers reaches about 100 $\mathrm{pT}/\sqrt{\mathrm{Hz}}$, and they are accurate to about 500 pT.

The most common magnetometers based on electron spin resonance (ESR) use vapors of alkali atoms [26], [29] or metastable ^{4}He atoms [30] confined in gas cells several centimeters in size. Atoms in vapor cells lose their spin coherence when they collide with the walls of the cell. To obtain long spin-coherence lifetimes, either the walls are coated with materials that preserve the spin coherence, such as paraffin [31], or a buffer gas is added to the cell that allows only slow diffusion of alkali atoms through the cell. Many ESR magnetometers are referred to as optical magnetometers, because the atoms are pumped [32] and interrogated [26] by light. For a recent review on optical magnetometry, see [6].

One example of an optical magnetometer is the Mx magnetometer [29], [33]. Here, the initial spin orientation is pumped by circularly polarized light. An oscillating magnetic field generated by a coil of wire resonantly drives the precession, which is detected as a modulation on a probe light field at the drive frequency. The drive frequency at which the resulting probe modulation is a maximum, is a measure of the Larmor frequency, and hence the magnetic field. The Mx magnetometer can be operated in a passive mode, in which an external oscillator generates the drive current and the frequency of this oscillator is locked to the Larmor resonance. Alternatively, the magnetometer can be operated in a self-oscillating mode [34], in which the optically detected precession signal is fed back directly to the drive coil, as shown in Fig. 4.

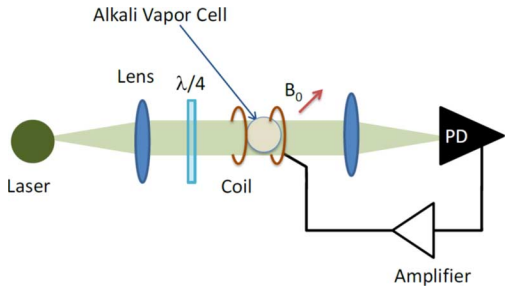

Fig. 4. Operation of an Mx magnetometer in the self-oscillating mode. Atoms contained in the vapor cell are optically pumped through use of circularly polarized light from a laser or lamp. An oscillating magnetic field generated by a coil drives a precession of the spins about the magnetic field B_0 when the drive frequency is tuned to the Larmor resonance. The modulation of the light intensity caused by the precession is detected with a photodiode (PD).

Most optical magnetometers have dead zones – orientations of the magnetic field with respect to the sensor axis that result in no signal. Furthermore, heading errors, small errors that depend on the orientation of the magnetic field with respect to the sensor axis, are often present. These can result from the nonlinear splitting of the Larmor frequency caused by the magnetic moment of the nucleus (nonlinear Zeeman shift), or from misalignment of the drive field axis from the probe field axis. Because metastable ^{4}He has no nuclear spin, ^{4}He magnetometers do not exhibit the nonlinear Zeeman shift and are therefore preferable when accuracy is important. Operation of the magnetometer in the Mz mode [34], in which the longitudinal, rather than transverse, reorientation of the atomic polarization is detected, further reduces the heading error.

Research on alkali magnetometers has seen a recent revival, in part due to the availability of inexpensive diode lasers that replace the lamps in many devices. Lasers have been used to efficiently pump higher order moments in the atoms [35]–[37] and also to create magnetically sensitive hyperfine coherence by use of only optical fields [38]–[40]. While all of these alkali magnetometers are subject to resonance broadening through spin-exchange collisions between the atoms, a new generation of so-called spin-exchange relaxation free (SERF) magnetometers [1], [41] has reached the highest sensitivities so far by suppressing this broadening in a regime dominated by interatomic collisions. With this method, sensitivities below 1 $\mathrm{fT}/\mathrm{Hz}^{1/2}$, similar to those of the best superconducting magnetometers, have been reached with DC [42] and RF [43] optical sensors. Borrowing (3) once again, the spin-projection noise limit of these magnetometers can be calculated, and for a potassium SERF magnetometer it is 3 $\mathrm{aT}/\mathrm{Hz}^{1/2}\mathrm{cm}^{3/2}$ [44]. This shows that there is still much room for improvement of atomic magnetometers, even when taking other noise sources into account, such as photon shot noise.

Commercial high-performance atomic magnetometers are used for applications in space, geophysics, and petroleum exploration. Biomagnetic fields such as those of the human heart [45] or brain [46] have been measured with laboratory prototypes of alkali magnetometers. Nuclear magnetic resonances [47] (NMR) and nuclear quadrupole resonances (NQRs) [48] have also be measured with optical magnetometers, and first steps toward low-field magnetic resonance imaging (MRI) using optical magnetometers have been taken [49], [50].

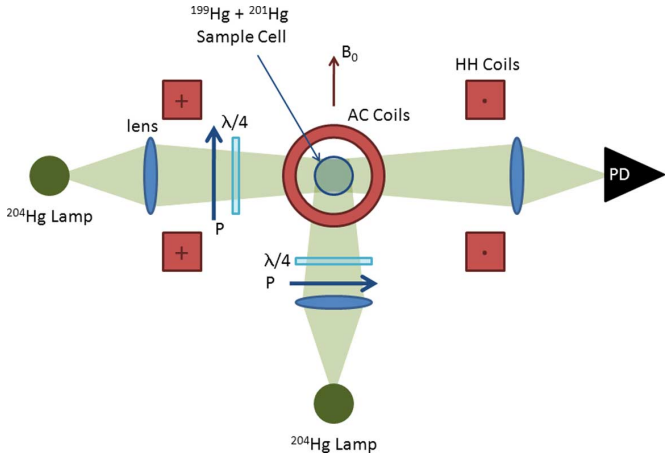

Fig. 5. Optically pumped NMR gyroscope. Atoms are optically pumped along a magnetic field B_0 by light from one $^{204}\mathrm{Hg}$ lamp. Light from a second $^{204}\mathrm{Hg}$ lamp reads out the nuclear Larmor precession signal, from which the rotation rate can be deduced. P refers to a polarizer and $\lambda/4$ to a quarter-wave plate.

While the sensitivity of alkali magnetometers generally degrades when the cell size is reduced [6], [51], chip-scale magnetometers have reached sensitivities below 5 $\mathrm{fT}/\mathrm{Hz}^{1/2}$ in cells of 1 mm thickness [52]. Magnetometers that have a sensitivity below the standard quantum limit have also been realized. On time scales shorter than the relaxation period sensitivities have been improved in cold atoms [53] as well as in hot vapors [54] and the use of quantum nondemolition measurements has resulted in a larger bandwidth for DC magnetometers [55]. Even smaller atomic ensembles are used in magnetometers based on Bose–Einstein condensates of only 120 $\mu\mathrm{m}^2$ that demonstrated sensitivities of 8.3 $\mathrm{pT}/\mathrm{Hz}^{1/2}$ [56].

IV. NMR Gyroscopes

Nuclear magnetic resonance gyroscopes (NMRGs) detect rotation by measuring a corresponding shift in the Larmor precession frequency of nuclear spins in an applied magnetic field. When the NMRG is rotating about the axis of the static field B_0, the measured Larmor frequency is shifted by the rotation rate Ω:

$$\omega = \gamma B_0 + \Omega. \tag{4}$$

By monitoring the measured Larmor frequency while holding the static field constant, the rotation rate can be deduced.

One challenge implicit in NMR gyroscopes is how to stabilize the static magnetic field: a change in B_0 of $\sim 100\,\mathrm{fT}$ results in an apparent change in the rotation rate by $1\,^\circ/\mathrm{h}$, which is too large a drift for most navigation applications. This difficulty can be overcome by interrogating two isotopes, for example, $^{199}\mathrm{Hg}$ and $^{201}\mathrm{Hg}$, simultaneously. Because the two Hg isotopes have the same rotational shifts but different magnetic-field shifts, the dependence of the Larmor frequency on the static field can be removed [57], which allows for the determination of Ω independent of B_0 [57]–[60].

A simplified diagram of an NMR gyroscope based on mercury atoms is presented in Fig. 5 [57]. A vapor cell contains $^{199}\mathrm{Hg}$, $^{201}\mathrm{Hg}$, and a buffer gas. The Hg nuclear spins are optically pumped and probed with light at 253.7 nm emitted by two $^{204}\mathrm{Hg}$ lamps. Coherent spin precession at the atomic Larmor frequency is driven by applied AC magnetic fields perpendicular to a static field, B_0. The precession frequency is detected optically as a modulation of the probe-beam transmission.

Gyroscope performance is usually expressed in terms of the angle random walk (ARW) and bias instability. The ARW is a noise specification equal to the square root of the rate noise power spectral density, making the rate resolution of a gyroscope equal to $\delta\Omega_{\min} = \mathrm{ARW}/\sqrt{T}$. The bias instability is the minimum detectable rotation rate as determined by drift and low-frequency noise.

As of the early 1980s, the dual species NMRG approach based on Hg isotopes had achieved values of 0.05 $^\circ/\sqrt{\mathrm{h}}$ for the ARW [61] and bias instabilities of 0.02 $^\circ/\mathrm{h}$ [62]. Several reviews of this early work have been published [61]–[65].

Spin-exchange optical pumping (SEOP) [23] in mixtures of alkali and noble-gas atoms can also be used to realize NMRGs based on spin-polarized noble-gas nuclei [66]. Through SEOP, the alkali electronic spin polarization is transferred to the noble-gas nuclei through collisions. It is therefore possible to avoid use of ultraviolet light and instead optically pump the alkali atoms with near-infrared lasers or lamps. Beginning in the 1970s, NMRGs based on this approach were introduced [66], [67]. The alkali atoms that pumped the noble-gas nuclei were simultaneously used in an Mx magnetometer to sense noble-gas nuclear precession. These NMRGs achieved a bias instability near 0.01 $^\circ/\mathrm{h}$ and an ARW of 0.002 $^\circ/\sqrt{\mathrm{h}}$ [2].

Recently, a novel version of an NMR gyroscope based on a potassium-$^3\mathrm{He}$ comagnetometer was demonstrated that achieved an ARW of 0.002 $^\circ/\sqrt{\mathrm{h}}$ and a bias instability of 0.04 $^\circ/\mathrm{h}$ [68]. Operation of the system in a regime in which spin-exchange relaxation is strongly suppressed [41] (the SERF regime of Section III), allowed for very narrow resonance lines and correspondingly high sensitivity to rotation. A miniaturized NMRG based on a comagnetometer has also been proposed [69], similar to a previous design of a chip-scale atomic clock [70].

NMR gyroscopes have received renewed attention recently at least in part because of the advances made in chip-scale atomic clocks [71]. For some applications, NMR gyroscopes have the potential advantage over micromachined spinning or vibratory gyroscopes in that they contain no moving parts.

Many novel microfabrication techniques have been proposed and developed in the context of miniaturized NMRGs. A scheme was proposed [72] for using batch processing to develop a chip-scale NMRG. For low-power consumption, the device uses permanent magnets and vertical-cavity surface emitting lasers. Other proposals present details for cell microfabrication techniques for such devices [73], [74]. Another new proposal presents instrument geometries that make use of a diverging laser beam to simultaneously pump and probe the atoms and reduce common-mode noise through differential detection [75], [76]. Wafer-level arrays of glass blown spherical microcells have also been developed [77], [78] as have methods to deposit mirrors onto angled cell walls [79], [80]. A summary of components and integration methods can be found in [81].

On the basic physics side, [82] is a new proposal for using three noble-gas isotopes to allow the correction for NMR frequency shifts caused by the alkali polarization [83]. These shifts

TABLE II
MEASURED PERFORMANCE METRICS, INTERACTION TIMES, AND APPROXIMATE INSTRUMENT LENGTH SCALES FOR PUBLISHED ATOM INTERFEROMETERS. WE HAVE LIMITED THE REFERENCES TO PAPERS THAT PROVIDE SENSITIVITY MEASUREMENTS. THE LENGTH L INCLUDES THE LENGTHS OF THE STATE PREPARATION, INTERFEROMETRY, AND DETECTION REGIONS

Sensor Type	*Performance*		$2T$ [ms]	L [m]	*Reference*
	$\Delta g/g$ [1/Hz$^{1/2}$]				
	9.5×10^{-5}		20	0.3	[87]
	1.3×10^{-6}		100	0.3	[96]
Gravimeter	2.3×10^{-8}		320	0.5	[11, 97]
	1.4×10^{-8}		100	0.1	[98]
	8×10^{-9}		800	1.5	[90]
	1.7×10^{-7}		80	0.15	[99]
	2×10^{-4}		4	0.9	[100]
	2.6×10^{-4}		2.2	0.07	[101]
Gravity	dg/dz [(g/m)/Hz$^{1/2}$]				
Gradiometer	4×10^{-9}		60	1	[102]
	ARW [°/h$^{1/2}$]	Drift [°/h]			
	1.1×10^{-2}		1.3	2	[103]
	7×10^{-5}		7	2	[104]
Gyroscope	2×10^{-6}		7	2	[105]
	3×10^{-6}	7×10^{-5}	9	2	[89]
	7.5×10^{-4}	<1	60	0.3	[106]
	8.2×10^{-4}	2×10^{-3}	80	0.3	[107]
	0.7		4	0.9	[100]

depend on cell temperature and laser power and can ultimately limit the bias stability.

An NMR study on $^{129}\mathrm{Xe}$ and $^{131}\mathrm{Xe}$ nuclei has also been performed in a microfabricated cell of 1 mm^3 volume [84]. The nuclear quadrupolar shifts were particularly large in this system, which may present a challenge for microfabricated devices. These shifts arise from interactions between the atom's nuclear quadrupole moment and the electric-field gradient generated during wall collisions, and are present for all nuclei that have nuclear quadrupole moments [85]. In this study, the strong electric field gradient ($\sim$ 30 $\mathrm{GV/cm}^2$) was generated by anisotropy in the cell wall materials as opposed to the cell shape [86].

V. ATOM INTERFEROMETERS

Atom interferometry has grown explosively since the first atom-interferometric inertial sensors were demonstrated [87], [88], and the performance of gyroscopes [89] and gravimeters [90] based on atom interferometry now rivals the performance of the best inertial sensors of any kind. Several reviews of atomic interferometry have been published previously [14], [91]–[95]. Here, we focus on work that applies these instruments to precision inertial sensing. Table II is a summary of inertial sensors that have been demonstrated by use of atom interferometers, which demonstrates their evolution and current state of performance.

For all but one [103] of the atom interferometers in Table II, the atoms propagated in free space and the beamsplitters and reflectors were realized by momentum transfer with stimulated Raman transitions. Mechanical gratings have been used [103] and many other approaches have been investigated (for a review, see [95]). So far, light-pulse atom interferometers have achieved the highest performance. One notable alternative approach is to confine the atoms in optical or magnetic atom waveguides. In these systems, the momentum transfer to the atoms can be much larger and better controlled, which could potentially result in much larger interferometer areas [108]. Until now, most interferometers of this type have employed Bose–Einstein condensates as atom sources so that the atoms can be confined in the lowest-order spatial mode of the waveguide.

As with light, atom matter waves can be split and recombined to yield interference patterns, and can thus be used to perform sensitive interferometry measurements. Fig. 6 is a diagram of a Mach–Zehnder atom interferometer. An atomic beam is incident onto the interferometer from the left in state $|0\rangle$, indicated by a vector on the Bloch sphere pointing along $+z$. An optical beam splitter, created by a Raman pulse formed from two counterpropagating beams, results in a quantum superposition state for each atom such that it has equal probability to be in states $|0\rangle$ and $|1\rangle$ (state $|1\rangle$ is indicated by a vector on the Bloch sphere pointing along $-z$). At the same time, the Raman pulse imparts momentum $\hbar k_{\mathrm{eff}}$ to the wavepacket in state $|1\rangle$. After a period T, the wavepackets are intercepted by optical reflectors, again created by Raman pulses that simultaneously impart momentum kicks and cause the atoms to switch internal states. After another period T, a second beam splitter combines the two paths. The fraction of atoms emerging from the interferometer in states $|0\rangle$ and $|1\rangle$ depends on the difference between the accumulated phases in the interferometer arms, which depends on the fields from inertial forces that the atoms sense while in transit and the laser phases during the optical pulses [109].

In an interferometer optimized as a gravimeter, the stimulated Raman pulses are applied along and against the gravity vector. A phase shift proportional to the acceleration g of $\Delta\phi = -k_{\mathrm{eff}} g t^2$ accumulates over a time $t = 2T$. This phase shift causes a change in the ratio of state populations at the output of the interferometer, which can be measured to determine g.

When the atoms have an initial velocity orthogonal to the direction along which the stimulated Raman pulses are applied, then the wavepackets will spread apart and reconverge such that the interferometer paths enclose an area A. In this arrangement,

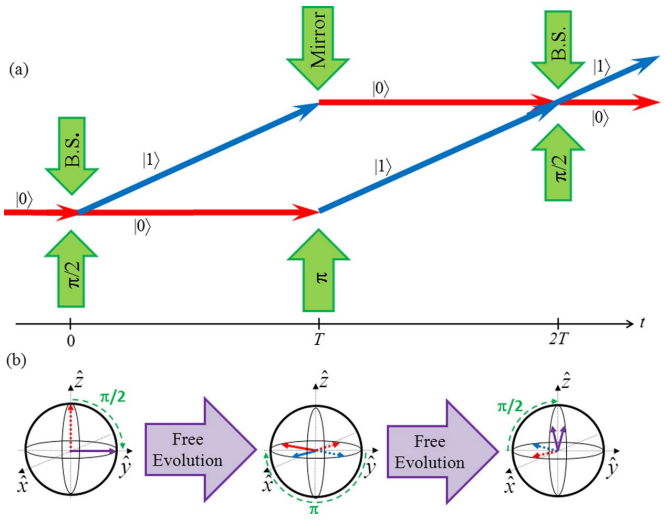

Fig. 6. A Mach–Zehnder atom interferometer. (a) Spatial representation of the interferometer. The light beams that form the $\pi/2$ and π pulses are represented by green arrows. Atoms that undergo the stimulated Raman transition change state and simultaneously receive a momentum kick of $\hbar(k_1 + k_2)$, where k_1 and k_2 are the wavevectors for the two beams that drive the transition. (b) Bloch-sphere representation. The first $\pi/2$ pulse creates a superposition of states $|0\rangle$ and $|1\rangle$. The two components of the superposition state take different interferometer paths, thus they are subject to different fields and acquire different phase shifts in the free evolution period. The final $\pi/2$ pulse writes the acquired phase onto the atomic state populations, which can be easily measured.

the interferometer is sensitive to rotations. Rotations cause a phase shift of $\Delta\phi = 4\pi\Omega\cdot\mathbf{A}/\lambda_{\rm dB}v = 2\,\Omega k_{\rm eff} v T^2$. Here $\lambda_{\rm dB} = h/p$ is the de Broglie wavelength, Ω is the rotation rate, and v is the atom velocity.

Because of the linear scaling of gyro phase shift with v, $\Delta\phi$ actually scales as $1/T$ with interaction period, whereas gravimeter sensitivity scales as $1/T^2$. This could partially explain why the most sensitive atom gyroscopes have been demonstrated with thermal atomic beams, while all of the best gravimeters have employed laser-cooled atoms. Gyroscope sensitivity is less dependent on atom velocity than gravimeter sensitivity, which can actually be seen in the sensitivity measurements in Table II. When plotted as a group versus T, the gravimeter sensitivity measurements scale very well with $1/T^2$. The scatter in the gyroscope sensitivities in Table II versus T is so large that the data is even consistent with having no interrogation time dependence, which suggests that noise sources that are not fundamental are more significant for gyroscopes than for gravimeters.

Atom interferometers have a potential advantage in sensitivity over light interferometers that arises because the de Broglie wavelength is typically more than four orders of magnitude smaller than the optical wavelength. For atom and light gyroscopes of the same area, small displacements cause much larger phase shifts for atoms and proportionally better sensitivity according to (2). The phase shift due to rotations for an atom interferometer is a factor of $\lambda_{h\nu}c/\lambda_{\rm dB}v \approx 10^{10}$ times larger than the phase shift for light interferometers of the same area, where $\lambda_{h\nu}$ is the light wavelength. The much larger response factors for atom interferometers more than makes up for their much smaller cross sectional areas and higher shot noise.

While the best sensitivity for gravimeters has been achieved with laser-cooled atoms in an atomic fountain [90], instruments based on dropped laser-cooled atoms have achieved competitive sensitivities in much smaller instruments [98], [99]. In [98], a six-beam magneto-optical trap (MOT) was loaded with atoms from a cold atomic beam, and the resulting cold atom cloud was dropped and interrogated in free fall. In [99], the atoms were directly laser-cooled in a pyramidal MOT and interrogated with the same single laser beam, and the apparatus is dramatically simpler than other approaches.

All of these interferometers potentially suffer from the inability to distinguish phase shifts from platform vibrations from phase shifts from inertial forces. Gravity gradiometers, which measure gravity gradients, can potentially overcome this shortcoming by canceling out platform vibrations by use of two gravimeters mounted to the same reference frame [102].

The best performing atomic gyroscope has been demonstrated with thermal cesium atomic beams. Since such an interferometer is sensitive to accelerations and rotations, large improvements over the initial sensitivity were achieved by use of differential measurements with counterpropagating atomic beams [105]. The rotation signals from counterpropagating beams have the opposite sign, whereas the acceleration signals have the same sign. Taking the signal sums and differences can yield both acceleration and rotation measurements from the same instrument [89], [106], [107].

Inertial sensors based on atom interferometers are already surpassing the sensitivity of most other routinely deployed high-performance inertial instruments.[1] Ring laser gyroscopes typically achieve a rotation rate sensitivity of about $3\times10^{-3}\ ^\circ/\sqrt{\rm h}$ and a bias stability of about $3\times10^{-3}\ ^\circ/{\rm h}$.[2] The performance reported in [89] (see Table II) exceeds these by factors of 1000 and 40, respectively. While atom interferometer gyroscopes are not commercially available at the time of this writing, it appears likely that commercial instruments will be available in the near future.

VI. Other Atomic Sensors

Laser-cooled cesium and rubidium atoms have been used to perform absolute measurements of microwave power in microwave waveguides [110], [111]. Measurements of the incident power agree with conventional microwave power measurements at the level of a few percent.

Electric fields can also be measured with high sensitivity by use of atomic vapors. Typically, Rydberg atoms [112] are used because their large electric dipole moment leads to correspondingly large frequency shifts of the atomic levels with electric field [113]. Frequency shifts can be measured by use of microwave [113] or laser [12] spectroscopy. Electric field sensitivities in the range of 10 $\mu{\rm V/cm}$ have been achieved with this technique [113].

[1]Several unique instruments such as the gyroscopes aboard Gravity Probe B and the C-II ring laser gyro in Christchurch, NZ still outperform atom interferometers. However, it appears unlikely that these heroic, highly specialized experiments will be replicated widely in the near future.

[2]See, for example, the Honeywell GG1320 Digital Laser Gyro. Reference is given for technical clarity and does not imply endorsement by NIST.

VII. Conclusion

We have described a number of inertial and physical sensors based on atomic spectroscopy and interferometry. Two broad classes of atomic sensors can be defined: those based on room-temperature atoms confined in a vapor cell, and those based on laser-cooled atoms confined by optical and magnetic fields. At present, progress in magnetometry and electrometry is dominated by vapor cell techniques, while the best-performing gravimeters, gyroscopes, and clocks are based on laser-cooled atoms; we believe this trend is likely to continue for the foreseeable future.

Key application areas currently are those that require extreme sensitivity, and are simultaneously tolerant of a high degree of system complexity and high cost. These include geophysical surveys and ship and vehicle detection for atomic magnetometers, inertial navigation of aircraft, and ships for NMR gyroscopes, and precise gravitational field measurements on earth and in space for atom interferometers. Highly miniaturized versions of these instruments may increase the breadth of applications in which they are used and allow, for example, low-cost biomagnetic imaging, navigation of unmanned aerial vehicles, and perhaps even the detection of underground tunnels. We remain optimistic that research in this area will continue to evolve at a rapid pace and that new and important applications will continue to emerge.

Acknowledgment

This work is a contribution of the National Institute of Standards and Technology (NIST), an agency of the U.S. government, and is not subject to copyright.

References

[1] I. K. Kominis, T. W. Kornack, J. C. Allred, and M. V. Romalis, "A subfemtotesla multichannel atomic magnetometer," *Nature*, vol. 422, pp. 596–599, Apr. 2003.

[2] L. K. Lam, E. Phillips, E. Kanegsberg, and G. W. Kamin, "Application of CW single-mode GaAlAs lasers to Rb-Xe NMR gyroscopes," in *Proc. SPIE*, 1983, vol. 412, pp. 272–276.

[3] L. Allen and J. H. Eberly, *Optical Resonance and Two-Level Atoms*. New York: Wiley, 1975.

[4] W. Happer, "Optical pumping," *Rev. Mod. Phys.*, vol. 44, pp. 169–249, 1972.

[5] D. J. Wineland, J. J. Bollinger, W. M. Itano, and D. J. Heinzen, "Squeezed atomic states and projection noise in spectroscopy," *Phys. Rev. A*, vol. 50, pp. 67–88, 1994.

[6] D. Budker and M. Romalis, "Optical magnetometry," *Nature Phys.*, vol. 3, pp. 227–234, Apr. 2007.

[7] S. A. Diddams *et al.*, "An optical clock based on a single trapped Hg-$199(+)$ ion," *Science*, vol. 293, pp. 825–828, Aug. 2001.

[8] A. Clairon *et al.*, "A cesium fountain frequency standard – preliminary-results," *IEEE Trans. Instrum. Meas.*, vol. 44, no. 2, pp. 128–131, Apr. 1995.

[9] J. H. Shirley, W. D. Lee, and R. E. Drullinger, "Accuracy evaluation of the primary frequency standard NIST-7," *Metrologia*, vol. 38, pp. 427–458, 2001.

[10] E. B. Alexandrov and V. A. Bonchbruevich, "Optically pumped atomic magnetometers after 3 decades," *Opt. Eng.*, vol. 31, pp. 711–717, Apr. 1992.

[11] A. Peters, K. Y. Chung, and S. Chu, "High-precision gravity measurements using atom interferometry," *Metrologia*, vol. 38, pp. 25–61, 2001.

[12] A. K. Mohapatra, M. G. Bason, B. Butscher, K. J. Weatherill, and C. S. Adams, "A giant electro-optic effect using polarizable dark states," *Nature Phys.*, vol. 4, pp. 890–894, 2008.

[13] J. Vanier and C. Audoin, *The Quantum Physics of Atomic Frequency Standards*. New York: Adam Hilger, 1992.

[14] C. J. Borde, "Atomic clocks and inertial sensors," *Metrologia*, vol. 39, pp. 435–463, 2002.

[15] M. A. Kasevich, E. Riis, S. Chu, and R. G. Devoe, "Rf spectroscopy in an atomic fountain," *Phys. Rev. Lett.*, vol. 63, pp. 612–616, Aug. 1989.

[16] A. Clairon, C. Salomon, S. Guellati, and W. D. Phillips, "Ramsey resonance in a Zacharias fountain," *Europhys. Lett.*, vol. 16, pp. 165–170, Sep. 1991.

[17] J. Guena *et al.*, "Demonstration of a dual alkali Rb/Cs fountain clock," *IEEE Trans. Ultrason., Ferroelectr. Freq. Control,* , vol. 57, no. 3, pp. 647–653, Mar. 2010.

[18] L. Hollberg *et al.*, "Optical frequency standards and measurements," *IEEE J. Quantum Electron.*, vol. 37, no. 12, pp. 1502–1513, Dec. 2001.

[19] T. Rosenband *et al.*, "Frequency ratio of Al+ and Hg+ single-ion optical clocks; Metrology at the 17th decimal place," *Science*, vol. 319, pp. 1808–1812, Mar. 2008.

[20] A. D. Ludlow *et al.*, "Sr lattice clock at $1 \times 10(-16)$ fractional uncertainty by remote optical evaluation with a Ca clock," *Science*, vol. 319, pp. 1805–1808, Mar. 2008.

[21] S. J. Smullin, I. M. Savukov, G. Vasilakis, R. K. Ghosh, and M. V. Romalis, "Low-noise high-density alkali-metal scalar magnetometer," *Phys. Rev. A*, vol. 80, p. 033420, 2009.

[22] A. Kastler, "Les methodes optiques d'orientation atomique et leurs applications," in *Proc. Phys. Soc., Section A*, 1954, vol. 67, pp. 853–863.

[23] T. G. Walker and W. Happer, "Spin-exchange optical pumping of noble-gas nuclei," *Rev. Mod. Phys.*, vol. 69, pp. 629–642, Apr. 1997.

[24] I. I. Rabi, "Space quantization in a gyrating magnetic field," *Phys. Rev.*, vol. 51, pp. 652–654, 1937.

[25] W. E. Bell and A. L. Bloom, "Optically driven spin precession," *Phys. Rev. Lett.*, vol. 6, pp. 280–283, 1961.

[26] H. G. Dehmelt, "Modulation of a light beam by precessing absorbing atoms," *Phys. Rev.*, vol. 105, pp. 1924–1925, 1957.

[27] G. S. Waters and P. D. Francis, "A nuclear magnetometer," *J. Sci. Instrum.*, vol. 35, pp. 88–93, 1958.

[28] A. W. Overhauser, "Polarization of nuclei in metals," *Phys. Rev.*, vol. 92, p. 411, 1953.

[29] W. E. Bell and A. Bloom, "Optical detection of magnetic resonance in alkali metal vapor," *Phys. Rev.*, vol. 107, pp. 1559–1565, 1957.

[30] R. E. Slocum and F. N. Reilly, "Low-field helium magnetometer for space applications," *IEEE Trans. Nucl. Sci.*, vol. NS-10, pp. 165–171, Jan. 1963.

[31] H. G. Robinson, E. S. Ensberg, and H. G. Dehmelt, "Preservation of a spin state in free atom-inert surface collisions," *Bull. Amer. Phys. Soc.*, vol. 3, p. 9, 1958.

[32] A. Kastler, "Production et detection optique d'une inegalite de population," *J. Phys. Radium*, vol. 11, pp. 255–265, 1950.

[33] S. Groeger, G. Bison, J. L. Schenker, R. Wynands, and A. Weis, "A high-sensitivity laser-pumped M-x magnetometer," *Eur. Phys. J. D*, vol. 38, pp. 239–247, May 2006.

[34] A. Bloom, "Principles of operation of the Rubidium vapor magnetometer," *Appl. Opt.*, vol. 1, pp. 61–68, 1962.

[35] D. Budker, D. F. Kimball, S. M. Rochester, V. V. Yashchuk, and M. Zolotorev, "Sensitive magnetometry based on nonlinear magneto-optical rotation," *Phys. Rev. A*, vol. 62, p. 043403, Oct. 2000.

[36] D. Budker, D. F. Kimball, V. V. Yashchuk, and M. Zolotorev, "Nonlinear magneto-optical rotation with frequency-modulated light," *Phys. Rev. A*, vol. 65, p. 055403, May 2002.

[37] H. Gilles, B. Cheron, and J. Hamel, "He-4 optical-pumping with polarization modulated light and magnetometry application," *J. De Physique IV*, vol. 1, pp. 489–492, 1991.

[38] E. B. Aleksandrov, A. B. Mamyrin, and A. P. Naumov, "Hfs-magnetometer for absolute measurement of magnetic induction of weak magnetic-fields," *Meas. Tech.*, vol. 20, pp. 1048–1051, 1977.

[39] M. Stahler, S. Knappe, C. Affolderbach, W. Kemp, and R. Wynands, "Picotesla magnetometry with coherent dark states," *Europhys. Lett.*, vol. 54, pp. 323–328, May 2001.

[40] E. B. Aleksandrov, M. V. Balabas, A. K. Vershovskii, and A. S. Pazgalev, "A new model of a quantum magnetometer: A single-cell Cs-K tandem based on four-quantum resonance in K-39 atoms," *Tech. Phys.*, vol. 45, pp. 931–936, 2000.

[41] J. C. Allred, R. N. Lyman, T. W. Kornack, and M. V. Romalis, "High-sensitivity atomic magnetometer unaffected by spin-exchange relaxation," *Phys. Rev. Lett.*, vol. 89, p. 130801, 2002.

[42] H. B. Dang, A. C. Maloof, and M. V. Romalis, "Ultra-high sensitivity magnetic field and magnetization measurements with an atomic magnetometer," *Appl. Phys. Lett.*, vol. 97, p. 151110, 2010.

[43] T. Fernholz *et al.*, "Spin squeezing of atomic ensembles via nuclear-electronic spin entanglement," *Phys. Rev. Lett.*, vol. 101, p. 173601, 2008.

[44] I. M. S. S. Savukov, M. V. Romalis, and K. L. Sauer, "Tunable atomic magnetometer for detection of radio-frequency magnetic fields," *Phys. Rev. Lett.*, vol. 95, p. 063004, 2005.

[45] G. Bison, R. Wynands, and A. Weis, "A laser-pumped magnetometer for the mapping of human cardiomagnetic fields," *Appl. Phys. B*, vol. 76, pp. 325–328, Mar. 2003.

[46] H. Xia, A. B.-A. Baranga, D. Hoffman, and M. V. Romalis, "Magnetoencephalography with an atomic magnetometer," *Appl. Phys. Lett.*, vol. 89, p. 211104, 2006.

[47] I. M. Savukov and M. V. Romalis, "NMR detection with an atomic magnetometer," *Phys. Rev. Lett.*, vol. 94, p. 123001, Apr. 2005.

[48] S.-K. Lee, K. L. Sauer, S. J. Seltzer, O. Alem, and M. V. Romalis, "Subfemtotesla radio-frequency atomic magnetometer for detection of nuclear quadrupole resonance," *Appl. Phys. Lett.*, vol. 89, p. 214106, 2006.

[49] I. M. Savukov *et al.*, "MRI with an atomic magnetometer suitable for practical imaging applications," *J. Magn. Reson.*, vol. 199, pp. 188–191, Aug. 2009.

[50] S. J. Xu *et al.*, "Magnetic resonance imaging with an optical atomic magnetometer," in *Proc. Nat. Acad. Sci. United States of America*, Aug. 2006, vol. 103, pp. 12668–12671.

[51] V. Shah, S. Knappe, P. D. D. Schwindt, and J. Kitching, "Sub-picotesla atomic magnetometry with a microfabricated vapor cell," *Nature Photonics*, vol. 1, pp. 649–652, 2007.

[52] W. C. Griffith, S. Knappe, and J. Kitching, "Femtotesla atomic magnetometry in a microfabricated vapor cell," *Opt. Exp.*, vol. 18, pp. 27167–27172, 2010.

[53] M. Koschorreck, M. Napolitano, B. Dubost, and M. W. Mitchell, "Quantum nondemolition measurement of large-spin ensembles by dynamical decoupling," *Phys. Rev. Lett.*, vol. 105, p. 093602-4, 2010.

[54] W. Wasilewski *et al.*, "Quantum noise limited and entanglement-assisted magnetometry," *Phys. Rev. Lett.*, vol. 104, p. 133601, 2010.

[55] V. Shah, G. Vasilakis, and M. V. Romalis, "High bandwidth atomic magnetometery with continuous quantum nondemolition measurements," *Phys. Rev. Lett.*, vol. 104, p. 013601, Jan. 2010.

[56] M. Vengalattore *et al.*, "High-resolution magnetometry with a spinor Bose-Einstein condensate," *Phys. Rev. Lett.*, vol. 98, p. 200801, May 2007.

[57] J. H. Simpson, J. T. Fraser, and I. A. Greenwood, "An optically pumped NMR resonance gyroscope," *IEEE Trans. Aerosp.*, vol. 1, pp. 1107–1110, 1963.

[58] J. H. Simpson, "Nuclear gyroscopes," *Astronautics and Aeronautics*, vol. 2, pp. 42–48, 1964.

[59] D. S. Bayley, I. A. J. Greenwood, and J. J. H. Simpson, "Optically pumped nuclear magnetic resonance gyroscope," U.S. Patent 3,778,700, Dec. 11, 1973.

[60] I. A. Greenwood and J. H. Simpson, "Fundamental noise limitations in magnetic resonance gyroscopes," in *Proc. IEEE Nat. Aerosp. Electron. Conf.*, 1977, pp. 1246–1250.

[61] F. A. Karwacki, "Nuclear magnetic resonance gyro development," *J. Inst. Navigation*, vol. 27, pp. 72–78, 1980.

[62] M. M. Kuritsky *et al.*, "Inertial navigation," *Proc. IEEE*, vol. 71, pp. 1156–1176, 1983.

[63] K. F. Woodman, P. W. Franks, and M. D. Richards, "The nuclear magnetic resonance gyroscope – A review," *The Journal of Navigation*, vol. 40, pp. 366–384, 1987.

[64] K. Liu *et al.*, "The development of micro-gyroscope technology," *J. Micromech. Microeng.*, vol. 19, p. 113001, 2009.

[65] E. A. Donley, "Nuclear magnetic resonance gyroscopes," in *Proc. IEEE Sensors*, Waikaloa, HI, 2010, pp. 17–22.

[66] E. Kanegsberg, "A nuclear magnetic resonance (NMR) gyro with optical magnetometer detection," in *Proc. SPIE*, 1978, vol. 157, pp. 73–80.

[67] B. C. Grover, E. Kanegsberg, J. G. Mark, and R. L. Meyer, "Nuclear magnetic resonance gyro," U.S. Patent 4,157,495, 1979.

[68] T. W. Kornack, R. K. Ghosh, and M. V. Romalis, "Nuclear spin based gyroscope based on an atomic comagnetometer," *Phys. Rev. Lett.*, vol. 95, p. 230801, Dec. 2005.

[69] L. Lust and D. W. Youngner, "Chip scale atomic gyroscope," U.S. Patent 7,359,059, Apr. 15, 2008.

[70] D. W. Youngner *et al.*, "A manufacturable chip-scale atomic clock," in *Proc. IEEE Transducers '07 & Eurosensors XXI Conf.*, Lyon, France, 2007, pp. 39–44.

[71] S. Knappe, "MEMS atomic clocks," in *Comprehensive Microsystems*, Y. Gianchani, Ed. *et al.* Maryland Heights, MO: Elsevier, 2007, vol. 3, pp. 571–612.

[72] H. C. Abbink, E. Kanegsberg, and R. A. Patterson, "NMR Gyroscope," U.S. Patent 7,239,135, Jul. 3, 2007.

[73] H. C. Abbink, E. Kanegsberg, K. D. Marino, and C. H. Volk, "Microcell for NMR gyroscope," U.S. Patent 7,292,031, Nov. 6, 2007.

[74] H. C. Abbink, W. P. Debley, C. E. Geosling, D. K. Sakaida, and R. E. Stewart, "Middle layer of die structure that comprises a cavity that holds an alkali metal," U.S. Patent 7,292,111, Nov. 6, 2007.

[75] J. Kitching, E. A. Donley, E. Hodby, A. Shkel, and J. Eklund, "Compact atomic magnetometer and gyroscope based on a diverging laser beam," U.S. Patent 7,872,473 B2, Jan. 18, 2011.

[76] E. Hodby, E. A. Donley, and J. Kitching, "Differential atomic magnetometry based on a diverging laser beam," *Appl. Phys. Lett.*, vol. 91, pp. 011109–3, 2007.

[77] E. J. Eklund, A. M. Shkel, S. Knappe, E. Donley, and J. Kitching, "Glass-blown spherical microcells for chip-scale atomic devices," *Sens. Actuators A*, vol. 143, pp. 175–180, 2008.

[78] E. J. Eklund, A. M. Shkel, S. Knappe, E. Donley, and J. Kitching, "Glass-blown spherical microcells for chip-scale atomic devices," *Sens. Actuators A*, vol. 16, pp. 232–239, 2007.

[79] M. A. Perez *et al.*, "Rubidium vapor cell with integrated Bragg reflectors for compact atomic MEMS," *Sens. Actuators A*, vol. 154, pp. 295–303, 2009.

[80] M. A. Perez, J. Kitching, and A. M. Shkel, "Design and demonstration of PECVD multilayer dielectric mirrors optimized for micromachined cavity angled sidewalls," *Sens. Actuators A*, pp. 23–32, 2009.

[81] E. J. Eklund, "Microgyroscope based on spin-polarized nuclei," Ph.D. dissertation, Dept. Mech. Eng., Univ. California, Irvine, CA, 2008.

[82] E. Kanegsberg, "Nuclear magnetic resonance gyroscope," U.S. Patent 7,282,910 B1, Oct. 16, 2007.

[83] N. R. Newbury *et al.*, "Polarization-dependent frequency-shifts from Rb-He-3 collisions," *Phys. Rev. A*, vol. 48, pp. 558–568, Jul. 1993.

[84] E. A. Donley *et al.*, "Nuclear quadrupole resonances in compact vapor cells: The crossover between the NMR and the nuclear quadrupole resonance interaction regimes," *Phys. Rev. A*, vol. 79, p. 013420, 2009.

[85] C. Cohen-Tannoudji, "Relaxation quadrupolaire de l'isotope 201Hg sur des parois de quartz," *J. De Physique*, vol. 24, pp. 653–660, 1963.

[86] Z. Wu, W. Happer, and J. M. Daniels, "Coherent nuclear-spin interactions of adsorbed Xe-131 gas with surfaces," *Phys. Rev. Lett.*, vol. 59, pp. 1480–1483, Sep. 1987.

[87] M. Kasevich and S. Chu, "Atomic interferometry using stimulated Raman transitions," *Phys. Rev. Lett.*, vol. 67, pp. 181–184, Jul. 1991.

[88] F. Riehle, T. Kisters, A. Witte, J. Helmcke, and C. J. Borde, "Optical Ramsey spectroscopy in a rotating frame – Sagnac effect in a matter-wave interferometer," *Phys. Rev. Lett.*, vol. 67, pp. 177–180, Jul. 1991.

[89] D. S. Durfee, Y. K. Shaham, and M. A. Kasevich, "Long-term stability of an area-reversible atom-interferometer sagnac gyroscope," *Phys. Rev. Lett.*, vol. 97, p. 240801, 2006.

[90] H. Muller, S. W. Chiow, S. Herrmann, S. Chu, and K. Y. Chung, "Atom-interferometry tests of the isotropy of post-Newtonian gravity," *Phys. Rev. Lett.*, vol. 100, p. 031101, 2008.

[91] P. Berman, *Atom Interferometry*. New York: Academic Press, 1997.

[92] M. A. Kasevich, "Coherence with atoms," *Science*, vol. 298, pp. 1363–1368, Nov. 2002.

[93] A. Miffre, M. Jacquey, M. Buchner, G. Trenec, and J. Vigue, "Atom interferometry," *Physica Scripta*, vol. 74, pp. C15–C23, Aug. 2006.

[94] M. de Angelis *et al.*, "Precision gravimetry with atomic sensors," *Meas. Sci. Technol.*, vol. 20, p. 022001, 2009.

[95] A. D. Cronin, J. Schmiedmayer, and D. E. Pritchard, "Optics and interferometry with atoms and molecules," *Rev. Mod. Phys.*, vol. 81, pp. 1051–1129, Jul.-Sep. 2009.

[96] M. Kasevich and S. Chu, "Measurement of the gravitational acceleration of an atom with a light-pulse atom interferometer," *Appl. Phys. B-Photophys. Laser Chem.*, vol. 54, pp. 321–332, May 1992.

[97] A. Peters, K. Y. Chung, and S. Chu, "Measurement of gravitational acceleration by dropping atoms," *Nature*, vol. 400, pp. 849–852, Aug. 1999.

[98] J. L. Gouet *et al.*, "Limits to the sensitivity of a low noise compact atomic gravimeter," *Appl. Phys. B-Lasers Opt.*, vol. 92, pp. 133–144, 2008.

[99] Q. Bodart *et al.*, "A cold atom pyramidal gravimeter with a single laser beam," *Appl. Phys. Lett.*, p. 134101, 2010.

[100] T. Müller *et al.*, "A compact dual atom interferometer gyroscope based on laser-cooled rubidium," *Euro. Phys. J. D*, vol. 53, pp. 273–281, 2009.

[101] D. L. Butts, J. M. Kinast, B. P. Timmons, and R. E. Stoner, "Light pulse atom interferometry at short interrogation times," *J. Opt. Soc. Amer. B*, vol. 28, pp. 416–421, 2011.
[102] J. M. McGuirk, G. T. Foster, J. B. Fixler, M. J. Snadden, and M. A. Kasevich, "Sensitive absolute-gravity gradiometry using atom interferometry," *Phys. Rev. A*, vol. 65, p. 033608, 2002.
[103] A. Lenef *et al.*, "Rotation sensing with an atom interferometer," *Phys. Rev. Lett.*, vol. 78, pp. 760–763, 1997.
[104] T. L. Gustavson, P. Bouyer, and M. A. Kasevich, "Precision rotation measurements with an atom interferometer gyroscope," *Phys. Rev. Lett.*, vol. 78, pp. 2046–2049, Mar. 1997.
[105] T. L. Gustavson, A. Landragin, and M. A. Kasevich, "Rotation sensing with a dual atom-interferometer Sagnac gyroscope," *Classical and Quantum Gravity*, vol. 17, pp. 2385–2398, Jun. 2000.
[106] B. Canuel *et al.*, "Six-axis inertial sensor using cold-atom interferometry," *Phys. Rev. Lett.*, vol. 97, p. 010402, Jul. 2006.
[107] A. Gauguet, B. Canuel, T. Leveque, W. Chaibi, and A. Landragin, "Characterization and limits of a cold-atom Sagnac interferometer," *Phys. Rev. A*, vol. 80, p. 163604, 2009.
[108] Y. J. Wang *et al.*, "Atom Michelson interferometer on a chip using a Bose-Einstein condensate," *Phys. Rev. Lett.*, vol. 94, p. 090405, Mar. 2005.
[109] C. Antoine and C. J. Borde, "Quantum theory of atomic clocks and gravito-inertial sensors: An update," *J. Opt. B: Quantum Semiclass. Opt.*, vol. 5, pp. S199–S207, 2003.
[110] D. C. Paulusse, N. L. Rowell, and A. Michaud, "Accuracy of an atomic microwave power standard," *IEEE Trans. Instrum. Meas.*, vol. 54, no. 2, pp. 692–695, Apr. 2005.
[111] T. P. Crowley, E. A. Donley, and T. P. Heavner, "Quantum-based microwave power measurements: Proof-of-concept experiment," *Rev. Sci. Instrum.*, vol. 75, pp. 2575–2580, Aug. 2004.
[112] T. F. Gallagher, *Rydberg Atoms*. Cambridge, U.K.: Cambridge Univ. Press, 1994.
[113] A. Osterwalder and F. Merkt, "Using high Rydberg states as electric field sensors," *Phys. Rev. Lett.*, vol. 82, pp. 1831–1834, 1999.

John Kitching received the B.Sc. degree in physics from McGill University, Montreal, QC, Canada, in 1990 and the M.Sc. and Ph.D. degrees in applied physics from the California Institute of Technology, Pasadena, in 1995.

He is currently leads the Atomic Devices and Instrumentation Group in the Time and Frequency Division at the National Institute of Standards and Technology (NIST), Boulder, CO. His research interests include miniaturized instrumentation, atomic frequency standards, low-noise microwave oscillators, atomic magnetometers, and gyroscopes.

Svenja Knappe received the Diploma degree in physics in 1998 and the Ph.D. degree in 2001 from the University of Bonn, Bonn, Germany.

Since 2001, she has been pursuing research in the Time and Frequency Division, National Institute of Standards and Technology (NIST), Boulder, CO. Her research interests include precision laser spectroscopy, atomic clocks and atomic magnetometers, laser cooling, alkali vapor cell technology, applications of semiconductor lasers to problems in atomic physics and frequency control, and miniaturization of atomic spectroscopy.

Elizabeth Donley received the B.Sc. degree in physics from the University of Nevada, Las Vegas, in 1994, the M.Sc. degree in physics from the University of Colorado, Boulder, in 1996, and the Ph.D. degree in natural sciences from the Swiss Federal Institute of Technology, Zürich, in 2000. Her thesis research was on single-molecule spectroscopy at subkelvin temperatures.

Since 2002, she has been a Physicist in the Time and Frequency Division, National Institute of Standards and Technology (NIST), Boulder, where she has worked on the operation and development of atomic fountain clocks and on various chip scale atomic devices and instruments.